

Robust Nonlinear Model Predictive Control With Model Predictive Sliding Mode for Continuous-Time Systems

Elyse Hill

Intelligent and Cognitive Engineering (ICE)
Laboratory,
College of Engineering and Physical Sciences
(CEPS),
University of Guelph,
Guelph, ON N1G 2W1, Canada
e-mail: ehill06@uoguelph.ca

S. Andrew Gadsden¹

Associate Professor
Fellow ASME
ICE Laboratory,
Department of Mechanical Engineering,
McMaster University,
Hamilton, ON L8S 4L8, Canada
e-mail: gadsden@mcmaster.ca

Mohammad Biglarbegian

Associate Professor
Autonomous & Intelligent Control for Vehicles
Laboratory,
CEPS,
University of Guelph,
Guelph, ON N1G 2W1, Canada
e-mail: mbiglarb@uoguelph.ca

This paper presents a robust, tube-based nonlinear model predictive controller for continuous-time systems with additive disturbances which cascades two sampled-data model predictive controllers: the first creates a desired path using nominal dynamics, and the second maintains the true state close to the nominal state by regulating a sliding variable designed on the error between the true and nominal states. The sampled-data model predictive approach permits easy incorporation of continuous-time sliding mode dynamics, allowing a dynamic boundary layer and tube design to be included. In this way, the control applied to the system capitalizes on the robustness properties of traditional sliding mode control (SMC) while incorporating system constraints. Stability analysis is presented in the context of input-to-state stability (ISS) for continuous-time systems. The proposed controller is implemented on two case studies, is compared to benchmark tube-based model predictive controllers, and is evaluated using average root-mean-square (RMS) values on the state and input variables, in addition to average integral square error (ISE) and integral absolute error (IAE) values on the position states. Results reveal that the proposed technique responds to higher levels of disturbance with significant increases in control effort, eliminates constraint violation by using of constrained SMC as the secondary controller, and maintains similar tracking performance to benchmark controllers at lower levels of control effort. [DOI: 10.1115/1.4053026]

1 Introduction

Model predictive control (MPC) is a widely used control technique that formulates an optimal control effort over a time horizon for a system with respect to state and input constraints [1]. Because of its ability to control complex, multivariable systems with limited conceptual complexity, it has found success in the automotive and process control fields [2–5]. Though powerful, successful implementation of MPC depends on an explicit system model, without which it breaks down in the presence of disturbances, modeling error, or noise. In reality, all systems are plagued by uncertainties, motivating the development of robust MPC (RMPC) methods to maintain system performance in spite of uncertainty.

A popular robust method is tube-based RMPC, in which a nominal MPC problem generates a reference trajectory and a secondary controller endeavors to maintain the true system trajectory within a “tube” centered on the reference trajectory. Adherence to the tube is enforced by tightening the state and input constraints of the nominal MPC such that they are satisfied for all possible realizations of the given disturbances. Tube RMPC has been well studied for linear systems [6–9], and extensions to nonlinear systems have seen increased focus [10–13].

One prevalent approach in extensions to nonlinear systems in the literature has been to use sliding mode control (SMC) as the secondary controller. Because it rejects matched disturbances, SMC decreases the conservatism inherent in tube RMPC, which is traditionally designed on the worst possible realization of the disturbance. For example, the tube-based approach in Ref. [14] incorporates an SMC to reduce the effect of intersample disturbances afflicting a sampled-data nonlinear MPC (NMPC), designing the sliding surface to achieve the sliding mode at the initial

time instant. In a similar vein, Refs. [15–17] apply integral sliding mode to address matched and unmatched disturbances, first introduced in Ref. [18], allowing the nominal NMPC to be designed on a system without tightened constraints in the case of only matched disturbances and on a system with less conservative constraints in the case of unmatched disturbances. Further, a nonrigid tube technique is presented [19] that optimizes the tube geometry as a function of a time varying boundary layer, describing a relationship between the control bandwidth, system uncertainty, and tube size.

Though effective, these sliding mode based approaches fail to take into consideration system constraints in the design of their secondary controllers. This is especially true when implementing traditional SMC as in Refs. [14] and [19] because, where integral sliding mode can be naturally saturated by design through its controller gain, SMC must be saturated postdesign to adhere to actuator limitations. However, while input constraints can be reasonably considered by saturation, state constraints are typically disregarded, and adherence to them may be compromised by the introduction of input saturation [20]. Earlier research on this issue has focused on merging MPC and SMC control laws in a predictive scheme, as introduced in Ref. [21] with generalized predictive control, where the sliding variable is predicted along the horizon. Reference [22] implemented a receding horizon sliding mode for discrete-time systems designed to minimize the deviation of the sliding variable from zero. A recent approach by Rubagotti et al. [23] instead designed an MPC to mimic a discrete-time SMC, rather than merge the techniques into an explicit control law. Despite the fair amount of research in constrained SMC, literature on its unification with RMPC is scarce. To the best of our knowledge, only Ref. [24] has integrated MPC and SMC as an explicit control law within the context of tube RMPC, adding an integral SMC component to the optimal control problem. However, this approach is limited to linear systems, leaving room to investigate nonlinear solutions.

In this paper, we present a tube-based robust NMPC for nonlinear control affine systems with a constrained SMC. System dynamics are considered in continuous-time and controlled using

¹Corresponding author.

Contributed by the Dynamic Systems Division of ASME for publication in the JOURNAL OF DYNAMIC SYSTEMS, MEASUREMENT, AND CONTROL. Manuscript received May 13, 2021; final manuscript received November 5, 2021; published online December 27, 2021. Assoc. Editor: Huiping Li.

NMPC for sampled-data systems with piecewise-continuous control signals, as presented in Refs. [25] and [26]. The proposed scheme includes two cascaded NMPCs: one designed on the nominal system to create a reference trajectory, and one designed on the nominal system to minimize the distance between the true and nominal system trajectories.

The primary contribution of this work lies in the use and design of a constrained SMC as the latter controller, constructed as a sampled-data model predictive sliding mode controller (MPSMC), allowing an SMC to incorporate system constraints and mitigate performance loss. Contrary to the design in Ref. [24], the combination of MPC and SMC in this paper requires no linearization of system dynamics and no a priori constraint tightening. Asymptotic stability of the overarching control is proven through regional input-to-state stability (ISS) analysis. The controller is simulated on two case studies, and performance is evaluated using root-mean-squared values on the states and control effort.

The remainder of the paper is organized as follows: the notations used in this paper are presented in Sec. 2, followed by an outline of the problem statement in Sec. 3. Section 4 describes the proposed robust NMPC strategy. Section 5 examines the theoretical properties of the closed-loop system, followed by a discussion on simulation results in Sec. 6. Finally, the paper is concluded in Sec. 7.

2 Preliminaries and Notations

For any column vector $x \in \mathbb{R}^n$, $\|\cdot\|$ denotes the Euclidean norm, and $\|x\|_{\Pi}^2 := x^T \Pi x$, where Π is a symmetric matrix, is the weighted norm. Given two sets $A, B \subset \mathbb{R}^n$, and points $a \in A$ and $b \in B$, Minkowski set subtraction is defined as $A \ominus B := \{a \mid \{a\} \oplus B \subseteq A\}$, where \oplus describes set addition defined as $A \oplus B := \{a + b\}$. A set $\mathbb{R}_{\geq 0}$ is a set of non-negative real numbers. A class C^1 function is all continuously differentiable functions. A function $\gamma : \mathbb{R}_{\geq 0} \rightarrow \mathbb{R}_{\geq 0}$ belongs to class \mathcal{K} if it is continuous, $\gamma(0) = 0$, and strictly increasing. A function $\gamma : \mathbb{R}_{\geq 0} \rightarrow \mathbb{R}_{\geq 0}$ belongs to class \mathcal{K}_{∞} if it is a \mathcal{K} -function and $\gamma(s) \rightarrow \infty$ as $\lim_{s \rightarrow \infty}$. A function $\beta : \mathbb{R}_{\geq 0} \times \mathbb{R}_{\geq 0} \rightarrow \mathbb{R}_{\geq 0}$ belongs to a class \mathcal{KL} if it is continuous and if, for each fixed $t \geq 0$, $\beta(\cdot, t) \in \mathcal{K}$ and for each fixed $s \geq 0$, $\beta(s, \cdot)$ is nonincreasing and $\beta(s, t) \rightarrow 0$ as $t \rightarrow \infty$. Given $t_1 > 0$ and $t_2 > 0$, $\mathcal{L}([t_1, t_2], \mathbb{R})$ represents the Lebesgue measurable and essentially bounded functions mapping $u : [t_1, t_2] \rightarrow \mathbb{R}$.

3 Problem Setup

Consider a nonlinear, time-invariant, affine dynamic system with an additive disturbance

$$\dot{x}^{(n)}(t) = f(x(t)) + bu(t) + w(t) \quad (1)$$

where $x(t) \in \mathbb{R}^n$ is the system state with n th derivative, $u(t) \in \mathbb{R}^r$ is the system input, $w(t) \in \mathbb{R}^r$ is an external disturbance, and $b \in \mathbb{R}^{n \times r}$ is the input matrix. The vector field $f : \mathbb{R}^n \times \mathbb{R}^r \rightarrow \mathbb{R}^n$ is a C^1 function in its arguments and $f(0) = 0$, so that $(x, u) = (0, 0)$ is the equilibrium for the system if $w \equiv 0$. The solution to Eq. (1) at time t_1 for initial condition $x(t_1)$ and piecewise-continuous

control $u(\cdot) \in \mathcal{L}([t_1, t], \mathbb{R}^r)$ is denoted as $x(\tau; x(t_1), u(\cdot), w(\cdot))$, $\tau \in [t_1, t]$. In the absence of disturbances ($w = 0$), an undisturbed model with assumed dynamics $\hat{f} : \mathbb{R}^n \times \mathbb{R}^r \rightarrow \mathbb{R}^n$ is described by

$$\dot{x}^{(n)}(t) = \hat{f}(x(t)) + \hat{b}u(t) \quad (2)$$

For the remainder of the paper, we assume that no uncertainty exists in the input channel, such that $\hat{b} = b$. We consider for subsequent analysis that the systems of Eqs. (1) and (2) are feedback linearizable and can be described as a second-order nonlinear model with a single input (i.e., $n = 2, r = 1$) with states defined as $\zeta = [x \ \dot{x}]^T$. Further, all following analysis can be extended to multi-input systems, including square systems. Equation (1) is subject to constraints satisfying the following assumption:

ASSUMPTION 1. (State, input, and disturbance constraint sets) The constraint sets $\mathcal{X} \subseteq \mathbb{R}^n, \mathcal{U} \subseteq \mathbb{R}^r$, and $\mathcal{W} \subseteq \mathbb{R}^r$ are closed and bounded, containing the origin in their interior. Further, the external disturbance is bounded such that

$$w(t) \in \mathcal{W} := \{w \in \mathbb{R}^r : \|w\| \leq W\}, \quad \forall t \geq 0 \quad (3)$$

The control goal is to design a law to stabilize the closed-loop system subject to state and input constraints for any possible uncertainty upper bounded by W . In this paper, this is done using the tube-based RMPC method, wherein the control input to Eq. (1) is determined from: (1) an NMPC controller designed on Eq. (2) to compute nominal state and input trajectories $(z_{\text{MPC}}(t), v_{\text{MPC}}(t))$ along a horizon $[t_k, t_k + T]$ and (2) an auxiliary controller designed to maintain the true state $x(t)$ near $z_{\text{MPC}}(t)$. The total control for tube-based methodology is traditionally defined by

$$u(t) = v_{\text{MPC}}(t) + \kappa(x(t), z_{\text{MPC}}(t)) \quad (4)$$

where $x(t) \in \mathcal{X}, u(t) \in \mathcal{U}, v_{\text{MPC}}(t) \in \mathcal{V} \subseteq \mathcal{U}, z_{\text{MPC}}(t) \in \mathcal{Z} \subseteq \mathcal{X}$, and \mathcal{V}, \mathcal{Z} are tightened input and state constraints. The auxiliary controller $\kappa(x(t), z_{\text{MPC}}(t))$ steers the disturbed system trajectory toward the nominal system trajectory such that $x(t)$ remains inside a robust control invariant (RCI) set around $z_{\text{MPC}}(t)$.

DEFINITION 1. (Robust control invariant set) Let $e(t) := x(t) - z_{\text{MPC}}(t)$. A set $\mathcal{S} \subseteq \mathcal{X}$ is a RCI set if there exists a control $\kappa(x(t), z_{\text{MPC}}(t)) \in \mathcal{U}$ such that if $e(t_0) \in \mathcal{S}$, then for all allowable $w(t) \in \mathcal{W}$, it holds that $e(t) \in \mathcal{S} \quad \forall t \geq t_0$.

The set \mathcal{S} forms a bounded neighborhood (tube) around z_{MPC} , which can be rigid or nonrigid and determined offline or online. Determining \mathcal{S} depends on the selection of $\kappa(\cdot, \cdot)$, which will be discussed in Sec. 4.2.

4 Robust Nonlinear Model Predictive Control Framework

This section describes the proposed nonlinear tube-based NMPC, whose controller architecture is displayed in Fig. 1. The proposed framework is composed of two sampled-data model predictive controllers: an NMPC for the primary controller and an MPSMC for the auxiliary controller. In sampled-data NMPC, the optimal control problem is solved at sampling instances $t_k = kT_s$,

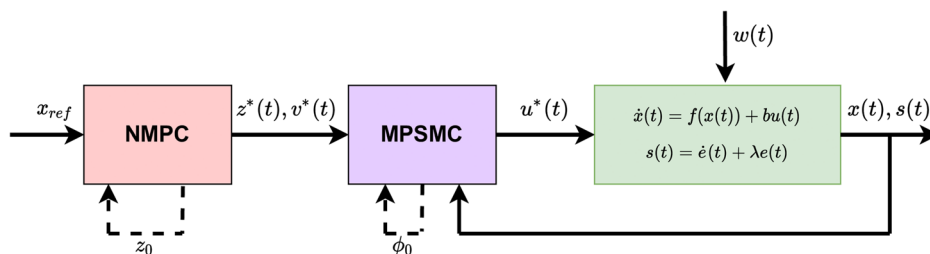


Fig. 1 Block diagram of the proposed control strategy

where $k \in \mathbb{N}$, and $T_s \in \mathbb{R}_{\geq 0}$ is the sampling time. We assume that the sampling time is constant such that $t_{k+1} = t_k + T_s$. Further, the cost functions satisfy the following:

ASSUMPTION 2. (Cost function continuity) The stage cost $l(\cdot, \cdot)$ is continuous, $l(0, 0) = 0$, and quadratic defined as $l(x, u) = \|x\|_Q^2 + \|u\|_R^2$, where Q is positive semidefinite, and R is positive definite. Further, the stage cost is lower bounded by a \mathcal{K}_∞ function α_l such that $\alpha_l(\|x(t)\|) \leq l(x, u)$, $\forall x(t) \in \mathcal{X}$, $u(t) \in \mathcal{U}$. The terminal cost $V_f(\cdot)$ is C^1 , $V_f(0) = 0$, and quadratic defined as $V_f(x) = \|x\|_P^2$, where P is positive definite.

4.1 Primary Controller (Nonlinear Model Predictive Control). The primary controller is designed to control the undisturbed system of Eq. (2) with nominal state $z(t)$ and nominal input $v(t)$. Its optimization problem at sampling instant t_k given initial state $z(t_k)$ is stated as:

Problem 1 (nominal optimal control problem).

$$\min_{v(\cdot) \in \mathcal{V}([t_k, t_k+T], \mathbb{R}^r)} J_{T, \text{nom}}(z(t_k), v(\cdot)) \quad (5a)$$

$$\text{subject to } \ddot{z}(\tau) = \hat{f}(z(\tau)) + bv(\tau) \quad (5b)$$

$$z(t_k) = z_0 \quad (5c)$$

$$z(\tau) \in \mathcal{Z}, \quad v(\tau) \in \mathcal{V} \quad (5d)$$

$$\begin{aligned} z(t_k + T) &\in \mathcal{Z}_f \\ \tau &\in [t_k, t_k + T] \end{aligned} \quad (5e)$$

where the initial state z_0 is selected as the solution to Eq. (2) with the optimal input determined by the controller at the previous sampling instant such that $z_0 = z^*(t_{k+1}; z(t_k), v^*(\cdot))$, where $(\cdot)^*$ denotes the optimal solution, and T is the time horizon. The constraint set $\mathcal{Z}_f \subset \mathcal{X}$ is the tightened terminal constraint set containing the origin in its interior. The open-loop cost function for the nominal state and input trajectories is

$$\begin{aligned} J_{T, \text{nom}}(z(t_k), v(\cdot)) &= \int_{t_k}^{t_k+T} l_{\text{nom}}(z(\tau), v(\tau)) d\tau + V_{f, \text{nom}}(z(t_k + T)) \end{aligned} \quad (6)$$

where the stage cost $l_{\text{nom}}(z, v) : \mathbb{R}^n \times \mathbb{R}^r \rightarrow \mathbb{R}_{\geq 0}$ is $l_{\text{nom}}(z, v) = \|z(\tau)\|_Q^2 + \|v(\tau)\|_R^2$; the terminal cost $V_{f, \text{nom}}(z) : \mathbb{R}^n \rightarrow \mathbb{R}_{\geq 0}$ is $V_{f, \text{nom}}(z) = \|z(t_k + T)\|_P^2$; and the subscript $(\cdot)_{\text{nom}}$ indicates the function belongs to the primary controller. The output of Eq. (5) is an optimal open-loop input sequence along the time horizon $v^*(\cdot; z(t_k))$. The control input that would be applied to the system until time instant t_{k+1} is denoted as

$$v_{\text{MPC}}(t) = v^*(t; z(t_k)), \quad t \in [t_k, t_{k+1}] \quad (7)$$

which is recalculated at each sampling instant. The associated optimal state to Eq. (7) is $z_{\text{MPC}}(t) = z^*(t; z(t_k), v^*(t; z(t_k)))$, $t \in [t_k, t_{k+1}]$. Note that the primary controller has no interaction with the real system as the state trajectory is initialized with nominal state z_0 . The goal of Problem 1 is to stabilize the undisturbed system. Given the above conditions, the closed-loop system for Eq. (2) based on the application of $u = v_{\text{MPC}}(t)$ is rendered stable given assumptions on the terminal ingredients:

ASSUMPTION 3. (Terminal set and terminal set stability) For the system given by Eq. (2), there exists a local asymptotically stabilizing control law $k_f(z) \in \mathcal{V}$ such that:

If $k_f(z) \in \mathcal{V} \quad \forall z \in \mathcal{Z}_f$, and if $z_0 \in \mathcal{Z}_f$, then the solution $z(t; z_0, k_f(z)) \in \mathcal{Z}_f, \forall t \geq 0$.

The terminal cost satisfies the inequalities

$$\alpha_3(\|z\|) \leq V_{f, \text{nom}}(z) \leq \alpha_4(\|z\|) \quad (8)$$

$$\begin{aligned} \frac{\delta V_{f, \text{nom}}(z)}{\delta z} (\hat{f}(z) + bk_f(z)) &\leq \\ -l_{\text{nom}}(z, k_f(z)), \forall z &\in \mathcal{Z}_f \end{aligned} \quad (9)$$

where $\alpha_3(\cdot), \alpha_4(\cdot) \in \mathcal{K}_\infty$.

These are standard assumptions to ensure stability of the closed-loop for Eq. (2) that are straightforward to satisfy given appropriate selection or design of $V_{f, \text{nom}}$. Based on selection of $V_{f, \text{nom}}$, the terminal constraint set \mathcal{Z}_f can also be determined as discussed in Refs. [1] and [26] and the references therein. Here, boundedness refers to the following definition:

DEFINITION 2. (Asymptotic ultimate boundedness) A system is asymptotically ultimately bounded if a set of initial conditions of the system converges asymptotically to a bounded set [11].

Remark 1. For simplicity, in this paper, we assume that the terminal constraints are limited either to a zero terminal constraint $\mathcal{Z}_f = \{0\}$ or to $\mathcal{Z}_f = \{z_e\}$ where z_e represents a set of equilibrium states specific to the system dynamics. Expansions to more robust terminal regions and sets are left as an avenue of future work.

4.2 Auxiliary Controller (Model Predictive Sliding Mode Controller).

The selected auxiliary controller is a model predictive sliding mode controller whose goal is to maintain the perturbed system of Eq. (1) near the undisturbed system of Eq. (2). In this paper, this is achieved by designing the MPSMC cost function to minimize the deviation between a system propagated using Eq. (2) and the optimal nominal trajectory $z^*(\cdot; z(t_k), v^*(\cdot; z(t_k)))$. Specifically, in recasting a sliding mode controller as a model predictive control problem, the control goal is to reach and maintain the sliding surface along the horizon. This is accomplished by incorporating the dynamics in the sliding mode, i.e., the dynamics that would maintain the derivative of the surface at zero. If a boundary layer is introduced, then direct parameterization of the RCI geometry is possible. Before deriving the auxiliary controller, we will first review the formulation of a boundary layer SMC as described in Ref. [27] and its relation to developing the tube \mathcal{S} . We assume the following on the system dynamics:

ASSUMPTION 4. The nonlinear dynamics are bounded by a model error function $F(x)$

$$|f(x) - \hat{f}(x)| \leq F(x) \quad (10)$$

The sliding surface (with time argument omitted) is defined as

$$s = \left(\frac{d}{dt} + \lambda \right)^{n-1} e_t = \dot{e}_t + \lambda e_t \quad (11)$$

where $e_t := x - x_d$ is the tracking error between the state and the desired trajectory, and $\lambda > 0$ is a scalar gain. The derivative of Eq. (11) is

$$\begin{aligned} \dot{s} &= \ddot{e}_t + \lambda \dot{e}_t \\ &= \dot{f}(x) + bu + w - \ddot{x}_d + \lambda \dot{e}_t \end{aligned} \quad (12)$$

As stated in Ref. [27], a boundary layer sliding mode controller (in the absence of disturbances) takes the form

$$u = b^{-1} \left[-\hat{f}(x) + \ddot{x}_d - \lambda \dot{e}_t - \bar{K}(x) \text{sat} \left(\frac{s}{\phi} \right) \right] \quad (13)$$

where $\text{sat}(\cdot)$ is the saturation function

$$\text{sat}(s, \phi) = \begin{cases} \frac{s}{\phi} & |s| \leq \phi \\ \text{sign}(s) & |s| > \phi \end{cases} \quad (14)$$

and where ϕ is the boundary layer thickness and the gain $\bar{K}(x)$ is determined by

$$\bar{K}(x) = F(x) + W + \eta - \dot{\phi} \quad (15)$$

where $\eta > 0$ is a design parameter that satisfies the sliding condition. A dynamic equation can be written for the boundary layer as

$$\dot{\phi} = -\lambda' \phi + F(x_d) + W + \eta \quad (16)$$

where λ' is the control bandwidth which can be used to tune ϕ . In sliding mode theory, the first three feedback terms of Eq. (13) are referred to as the equivalent control \hat{u} , which is the component of the input that maintains Eq. (12) at zero given known system dynamics. The last feedback term in Eq. (13) is referred to as the discontinuous control u_K , which is the component of the input that forces the system trajectories to the sliding surface. An RCI tube is formed for the state error vector $\zeta = [e_t \quad \dot{e}_t]^T$ from the time domain solution to Eq. (11)

$$\tilde{\zeta}(t) = e^{A(t-t_0)} \tilde{\zeta}(t_0) + \int_{t_0}^t e^{A(t-\tau)} B s(\tau) d\tau \quad (17)$$

where $A = -\lambda$ and $B = 1$ from the controllable canonical formulation. Taking the element-by-element absolute value of Eq. (17), noting $|s(\tau)| \leq \phi(\tau)$, and assigning $S(t) = |\tilde{\zeta}(t)|$, the tube is formally described by [19]

$$S(t) \leq e^{A(t-t_0)} S(t_0) + \int_{t_0}^t e^{A(t-\tau)} B \phi(\tau) d\tau \quad (18)$$

Equation (18) bounds the state tracking error and its derivatives as a function of the boundary layer thickness that bounds the sliding surface, rendering the sets

$$\mathcal{B} := \{s \in \mathbb{R}^n : |s(t)| \leq \phi(t), \forall x \in \mathcal{X}\} \quad (19)$$

$$\mathcal{S} := \{x \in \mathbb{R}^n : S(t) \leq e^{A(t-t_0)} S(t_0) + \int_{t_0}^t e^{A(t-\tau)} B \phi(\tau) d\tau, \forall x \in \mathcal{X}, \forall t \geq t_0\} \quad (20)$$

where \mathcal{B}, \mathcal{S} are RCI for the sliding surface and state error, respectively, by Definition 1.

The sliding mode problem presented above can be recast as a model predictive control problem subject to the definition of the sliding surface dynamics, system dynamics, and state and input constraints. The goal of the problem is to regulate $s = 0$, which is accomplished in sliding mode theory by driving Eq. (12) to zero. Given known system dynamics, this is accomplished by \hat{u} . However, the total control input u , necessary to achieve both the reaching and sliding phases, is the desired decision variable for the controller. The control u can be substituted into Eq. (12) by manipulating the relationship between u, \hat{u} , and u_K which is

$$u = \hat{u} + u_K \quad (21)$$

Rearranging for \hat{u} yields

$$\hat{u} = u - (-b^{-1} \bar{K}(x) \text{sat}(s, \phi)) \quad (22)$$

A new version of the sliding derivative for use in the optimal control problem is defined as

$$\dot{s} = f(x) + b(u + b^{-1} \bar{K}(x) \text{sat}(s, \phi)) - \ddot{x}_d + \lambda \dot{e}_t \quad (23)$$

Thus, the optimization for the auxiliary controller $\kappa(\cdot, \cdot)$ at time-step t_k is:

Problem 2 (auxiliary optimal control problem).

$$\min_{\hat{u}(\cdot) \in \mathcal{L}([t_k, t_k+T], \mathbb{R}^r)} J_{T,\kappa}(s(t_k), \hat{u}(\cdot)) \quad (24a)$$

$$\text{subject to } \dot{\hat{s}}(\tau) = \hat{f}(\hat{x}(\tau)) + b(\hat{u}(\tau)) \quad (24b)$$

$$+ b^{-1} \bar{K}(\hat{x}(\tau)) \text{sat}(\hat{s}(\tau), \hat{\phi}(\tau)) - \ddot{\hat{x}}_d(\tau) + \lambda \dot{\hat{e}}_t(\tau) \quad (24c)$$

$$\hat{\ddot{x}}(\tau) = \hat{f}(\hat{x}(\tau)) + b \hat{u}(\tau)$$

$$\dot{\hat{\phi}}(\tau) = -\lambda' \hat{\phi}(\tau) + F(x_d(\tau)) + W + \eta \quad (24d)$$

$$\dot{\hat{S}}(\tau) = A \hat{S}(\tau) + B \hat{\phi}(\tau) \quad (24e)$$

$$\hat{x}(t_k) = x(t_k), \quad \hat{s}(t_k) = s(t_k) \quad (24f)$$

$$\hat{\phi}(t_k) = \phi_0, \quad \hat{S}(t_k) = |e(t_k)| \quad (24g)$$

$$\hat{x}(\tau) \in \mathcal{X}, \quad \hat{u}(t) \in \mathcal{U} \quad (24h)$$

$$\hat{x}(t_k + T) \in \mathcal{X}_f, \quad \tau \in [t_k, t_k + T] \quad (24i)$$

where $x_d(\tau)$ and its derivatives are the associated optimal state trajectory from Problem 1, $\phi_0 = \hat{\phi}^*(t_{k+1}; s(t_k), \hat{u}^*(\cdot))$ from the previous sampling instant, and (\cdot) indicates internal variables in the optimization problem, specified to avoid confusion with the true system dynamics. The value $s(t_k)$ is dependent on the current state and the optimal nominal solution, evaluated using Eq. (11). The open-loop cost function, $J_{T,\kappa}$, of the predicted surface and input sequences is

$$J_{T,\kappa}(s(t_k), \hat{u}(\cdot)) = \int_{t_k}^{t_k+T} l_\kappa(\hat{s}(\tau), \hat{u}(\tau)) d\tau + V_{f,\kappa}(\hat{s}(t_k + T)) \quad (25)$$

where the stage cost $l_\kappa(s, u) : \mathbb{R}^r \times \mathbb{R}^r \rightarrow \mathbb{R}_{\geq 0}$ is $l_\kappa(s, u) = \|\hat{s}(\tau)\|_{Q'}^2 + \|\hat{u}(\tau)\|_{R'}^2$; the terminal cost $V_{f,\kappa}(s) : \mathbb{R}^r \rightarrow \mathbb{R}_{\geq 0}$ is $V_{f,\kappa}(s) = \|\hat{s}(t_k + T)\|_{P'}^2$; and the subscript $(\cdot)_{\kappa}$ indicates the function belongs to the auxiliary controller.

Remark 2. Given the model error function, $F(x)$, is an upper bound of possible parametric uncertainty, its presence in Eq. (24d) is justifiable despite the primary and auxiliary controllers being based on the same dynamics. However, if the true system dynamics $f(x)$ are known, one can eliminate the bound from the formulation.

The solution to Eq. (24) is the optimal open-loop control input implemented on the system until the next sampling instant t_{k+1}

$$u_{\text{MPC}}(t) = \hat{u}^*(t; s(t_k)), t \in [t_k, t_{k+1}] \quad (26)$$

Additional outputs of Eq. (24) are the associated predicted optimal trajectories for the sliding surface \hat{s}^* , the state trajectory \hat{x}^* , boundary layer thickness $\hat{\phi}^*$, and tube size \hat{S}^* for $t \in [t_k, t_k + T]$. The optimal tube size is the portion of the optimal tube trajectory implemented from the current time to the next sampling instant, i.e., $S_{\text{opt}}(t) = \hat{S}^*(t; s(t_k), \hat{u}^*(t; s(t_k))), t \in [t_k, t_{k+1}]$. This value is used to determine the tightened constraints. The inputs to Eq. (24) include the state, sliding variable, and state error of the real system at the current sampling instant, the previously optimized boundary layer size, and the optimal sequences $z^*(\cdot; z(t_k), v^*(\cdot; z(t_k)))$ and $v^*(\cdot; z(t_k))$ from the primary controller.

The nonlinear tube RMPC for the system in Eq. (1) formed by cascading Problems 1 and 2, as seen in Fig. 1 and as described in Algorithm 1, is referred to as NMPC-MPSMC for the remainder of the paper. As described in Algorithm 1, the control resulting from the MPSMC provides the total control to the disturbed system, supplanting the formulation in Eq. (4) such that the resultant closed-loop system at each sampling instant is

Algorithm 1: Robust Control Algorithm (NMPC-MPSMC)

Step 0:	At $t = t_0$, initialize $z(t_0) = \tilde{x}(t_0) = x(t_0) = x_{\text{ref}}(t_0)$ and $\tilde{s}(t_0) = s(t_0)$, where x_{ref} is the initial state of the reference trajectory
Step 1:	Solve Problem 1 to determine the optimal sequences $z^*(t)$, $v^*(t)$ at time t_k with current state $z(t_k)$
Step 2:	Solve Problem 2 to determine the optimal control $u^*(t)$, at time t_k with current state $x(t_k)$ and current sliding variable $s(t_k)$
Step 3:	Apply $u_{\text{MPC}}(t)$ to (1) during the interval $t \in [t_k, t_{k+1})$ and measure the successor variable $x(t_{k+1})$, $s(t_{k+1})$. Apply $u_{\text{MPC}}(t)$ to (2) and determine $z^*(t_{k+1})$.
Step 4:	Set $z(t_k) = z^*(t_{k+1})$, $\tilde{x}(t_k) = x(t_{k+1})$, $\tilde{s}(t_k) = s(t_{k+1})$, $t_k = t_{k+1}$ and go to Step 1.
Step 5:	Terminate at $t_{k+1} = t_f$, the final simulation time

$$\ddot{x}(t) = f(x(t)) + bu(t) + w(t), \quad u(t) = u_{\text{MPC}}(t) \quad (27)$$

Remark 3. Problem 2 assumes the same general formulation as Problem 1, but with respect to the sliding variable. As such, Assumption 3 can be redefined with the sliding dynamics:

ASSUMPTION 5. *There exists a stabilizing control law $k_f(x) \in \mathcal{U}$ such that:*

If $k_f(x) \in \mathcal{U}$, $\forall s \in \mathcal{B}$ and if $s(t_0) \in \mathcal{B}$, then $u = k_f(x)$ ensures $s(t; s(t_0), k_f(x)) \in \mathcal{B} \quad \forall t \geq t_0$.

The terminal cost satisfies the inequalities

$$\alpha_5(\|s(t)\|) \leq V_{f,k}(s(t)) \leq \alpha_6(\|s(t)\|) \quad (28)$$

$$\frac{\delta V_{f,k}(s(t))}{\delta s(t)}(\dot{s}(t)) \leq -I_\kappa(s(t), k_f(x)), \quad \forall s \in \mathcal{B} \quad (29)$$

where $\alpha_5(\cdot), \alpha_6(\cdot) \in \mathcal{K}_\infty$.

Assumption 5 reveals that due to the relationship established in Eq. (18), $s \in \mathcal{B} \rightarrow e \in \mathcal{S}$. Additionally, if $z_{\text{MPC}}(t) = 0$, then \mathcal{S} is control invariant for Eq. (1). Note that Eq. (29) can be used to verify the descent property of the value function for Problem 2, showing that the value function decreases along the solution trajectories from the first sampling instant, and thus that $s(t)$ decreases with respect to \mathcal{B} .

4.3 Constraint Tightening. The tightened constraints, which are necessary to ensure robust constraint satisfaction, are determined in this section. Constraints \mathcal{Z}, \mathcal{V} are initialized as equivalent to constraints \mathcal{X}, \mathcal{U} at time t_0 and change as a function of time based on the optimal tube size, $S_{\text{opt}}(t)$. The original constraints have the form

$$\mathcal{X} = \{x \in \mathbb{R}^n | L_x x \leq B_x\} \quad (30)$$

$$\mathcal{U} = \{u \in \mathbb{R}^r | L_u u \leq B_u\} \quad (31)$$

where L_x, L_u and B_x, B_u are user determined constants for the linear inequality constraints.

4.3.1 State Constraints. The state constraint can be tightened using the geometry of the tube determined by the auxiliary controller. Because applying Eq. (26) to Eq. (1) bounds the true state to an RCI, the difference between the nominal and true system trajectories is bounded as $x(t) - z_{\text{MPC}}(t) \in \mathcal{S}, \forall t \in [t_k, t_k + T]$. Rearranging yields the modified state constraint

$$\mathcal{Z} := \mathcal{X} \ominus \mathcal{S} \quad (32)$$

Resulting in the linear constraints $\mathcal{Z} = \{z \in \mathbb{R}^n : L_x z \leq B_x - L_x S_{\text{opt}}\}$.

4.3.2 Control Constraints. When an NMPC is used as the auxiliary control, control constraint tightening typically takes the form $\mathcal{V} = \gamma \mathcal{U}$, where the tightened constraint is a scalar fraction γ of the original constraint. However, in sliding mode based robust NMPC designs, the upper bound of the auxiliary control SMC is

used to tighten the input constraint. A similar approach is taken here with a basic assumption on the primary controller.

LEMMA 1. *Let the initial conditions of the nominal state $z(t)$ be such that Eq. (2) for the primary controller starts in the sliding mode. Then, the control necessary to maintain the sliding motion is the equivalent control \hat{u} and the tightened input constraint is*

$$\mathcal{V} := \mathcal{U} \ominus \{b^{-1} \bar{K}_{\max}(x(t))\} \quad (33)$$

where

$\bar{K}_{\max}(x(t)) = \max\{\bar{K}(z_{\text{MPC}}(t) - S_{\text{opt}}(t)), \bar{K}(z_{\text{MPC}}(t) + S_{\text{opt}}(t))\}, t \in [t_k, t_{k+1})$ represents the element-by-element maximum discontinuous control.

Proof. The upper bound of the controller input is the input constraint \mathcal{U} . By design this upper bounds the control allotted for Eq. (24), which includes both equivalent and discontinuous controls. In the sliding mode, only \hat{u} is necessary to maintain $\dot{s} = 0$. Thus, determining how much input should be allotted for \hat{u} can be reduced to maximizing the saturation term and subtracting it from the bound. The maximum discontinuous control becomes $\max\{u_K\} = \bar{K}(x(t))$, the value of which must be determined at the bounds of the tube defined as $x(t) = z_{\text{MPC}}(t) \pm S_{\text{opt}}(t)$, $t \in [t_k, t_{k+1})$. Substituting this information into Eq. (13) yields

$$\hat{u} \in \mathcal{U} \ominus \{b^{-1} \bar{K}_{\max}(x(t))\} \quad (34)$$

If $z(t_0) = x_{\text{ref}}(t_0)$, then the primary control starts in the sliding mode, only requires \hat{u} , and yields Eq. (33). This results in the tightened linear constraints $\mathcal{V} = \{v \in \mathbb{R}^r : L_u v \leq B_u - L_u b^{-1} \bar{K}_{\max}(x(t))\}$. ■

5 Stability Analysis

This section analyzes the feasibility of the auxiliary control and the convergence properties of the closed-loop system Eq. (27) using Eq. (26). Convergence is illustrated by way of input-to-state stability, which was introduced in Ref. [28] as a suitable framework to establish robust stability of MPC controlled systems and which is defined for continuous-time systems as:

DEFINITION 3. (Input-to-state stability) *Consider the system of Eq. (1) satisfying Assumption 1 and having initial condition $x_0 = x(t_0)$. Then, the system is ISS with respect to w if there exists functions $\beta \in \mathcal{K}\mathcal{L}, \sigma \in \mathcal{K}$ such that for all $t \geq t_0, x_0 \in \mathcal{X}$, bounded disturbance $w \in \mathcal{W}$, and bounded input $u \in \mathcal{U}$*

$$\|x(\tau; x_0, u(\cdot), w(\cdot))\| \leq \beta(\|x_0\|, t) + \sigma\left(\sup_{t_0 \leq \tau \leq t} \|w(\tau)\|\right), \quad \tau \in [t_0, t] \quad (35)$$

Given the above and the proposed control, the following stability results are stated.

THEOREM 1. *Suppose Assumptions 1–5 are satisfied and Problems 1 and 2 are feasible at the initial time instant. Then, the closed-loop system of Eq. (27) controlled by Eq. (26) is input-to-state stable with respect to $w(t) \in \mathcal{W}$ for all initial conditions $x(t_0) \in \mathcal{X}$.*

Remark 4. Because Problem 1 has no interaction with the disturbed system of Eq. (1), instead using the state and dynamics of the nominal system only, it is guaranteed recursively feasible and asymptotically ultimately bounded.

Proof. The proof of the theorem has two parts. First, recursive feasibility of Problem 2 is demonstrated, i.e., that existence of a solution at time t_k implies existence of a solution at t_{k+1} . Then, convergence of the closed-loop system in the sense of ISS is shown.

Feasibility: Assume the solution to Problem 2 exists at time t_k . The optimal input sequence solved at t_k can be written as a concatenation

$$\tilde{u}^*(\tau; s(t_k)) = \begin{cases} \tilde{u}^*(\tau; s(t_k)), & \tau \in [t_k, t_{k+1}] \\ \tilde{u}^*(\tau; s(t_k)), & \tau \in [t_{k+1}, t_k + T] \end{cases} \quad (36)$$

which satisfies the state and input constraints. By Assumption 5, at the next sampling instant t_{k+1} , there exists a feasible input \tilde{u} composed of the $\tau \in [t_{k+1}, t_k + T]$ portion of Eq. (36) and a $u = k_f(x)$ that satisfies control invariance for $s \in \mathcal{B}$ over $\tau \in [t_{k+1}, t_{k+1} + T]$

$$\tilde{u}(\tau; s(t_{k+1})) = \begin{cases} \tilde{u}^*(\tau; s(t_{k+1})), & \tau \in [t_{k+1}, t_k + T] \\ k_f(x(\tau)), & \tau \in [t_k + T, t_{k+1} + T] \end{cases} \quad (37)$$

Further, due to the RCI property associated with Problem 2, Eq. (37) guarantees that the true state will lie in the tube $\mathcal{S} \subseteq \mathcal{X}$, hence

$$x(t_{k+1} + \tau; \tilde{u}^*(\cdot), x(t_{k+1})) \in \mathcal{X}, \quad \forall \tau \in [0, T] \quad (38)$$

Because the sequence $\tilde{u}(\cdot; s(t_{k+1}))$ is admissible at the next sampling instant, feasibility at t_k implies feasibility at t_{k+1} , i.e., if Problem 2 is feasible at $t=0$, it is feasible for all $t \geq 0$.

Convergence: Problem 1 guarantees boundedness of Eq. (2) so there exists $\beta(\cdot) \in \text{KL}$ such that

$$\|z(t)\| \leq \beta(\|z(t_0)\|, t), \quad t \geq t_0 \quad (39)$$

Because Problem 2 induces an RCI for $e(t) \in \mathcal{S}$, we have a $\sigma(\cdot) \in \mathcal{K}$ such that

$$\|e(t)\| \leq \sigma\left(\sup_{t_0 \leq \tau \leq t} \|w(\tau)\|\right), \quad t \geq t_0 \quad (40)$$

Thus, using the definition $e(t) = x(t) - z(t)$, we can rearrange and apply the triangle inequality to get

$$\|x(t)\| \leq \|z(t)\| + \|e(t)\| \quad (41)$$

Substituting Eq. (39), Eq. (40), the bound of w from Eq. (3), and noting that the true and nominal systems are initialized the same, i.e., $x(t_0) = z(t_0)$

$$\|x(t)\| \leq \beta(\|x(t_0)\|, t) + \sigma(W) \quad (42)$$

So, the solution to Eq. (1) under the control of Eq. (26) is ISS in the closed-loop. ■

6 Numerical Examples

In this section, we verify the proposed method on two case studies and against two robust NMPC techniques. The first study involves control of a single input spring–mass–damper system, in which the effect of the disturbance bound and adherence to constraints are examined. The second application focuses on the control of a more complex multi-input spacecraft dynamic system, where sliding surface activity is inspected.

6.1 Case Study 1: Spring–Mass–Damper System. The proposed controller is verified on a nonlinear spring–mass–damper system, with dynamics given by Landis Markley and Crassidis [29] as

$$\dot{x}_1(t) = x_2(t) \quad (43a)$$

$$\dot{x}_2(t) = \frac{1}{m}(-k_1 x_1(t) - k_2 x_1^3(t) - c x_2(t)|x_2(t)| + u(t) + w(t)) \quad (43b)$$

where x_1 is the position of the mass with respect to equilibrium, x_2 is its velocity, u is the force applied to the mass, w is an additive load disturbance, and $m, k_1, k_2, c > 0$ are the mass, spring constants, and damping values, respectively. The value of w is randomized but satisfies $|w| \leq W$. The system $f(x)$ is

Table 1 System parameters: spring–mass–damper

Parameter	Value	Parameter	Value
k_1	1.5 N/m	λ	3
k_2	0.75 N/m	λ'	1
m	1 kg	x_0, z_0	$[0.5 \ 0]^T$ m
c	3 N s/m	Q, P	$\text{diag}(3 \ 3)$
W	0.25 N	R	1
η	0.25	Q', P'	10

Table 2 RMS values: spring–mass–damper

W = 0.25 N			
Controller			
Parameter	NMPC–NMPC [1]	NMPC–DTMPC [19]	NMPC–MPSMC
x_1 (m)	0.0945	0.111	0.0722
x_2 (m/s)	0.0530	0.0591	0.0533
u (N)	0.0635	0.0391	0.117
x_1 (m)	0.299	0.416	0.111
x_2 (m/s)	0.0589	0.0627	0.0629
u (N)	0.186	0.125	0.510

Table 3 x_1 integral errors: spring–mass–damper

Controller	W = 0.25 N	W = 1.25 N
ISE		
NMPC–NMPC [1]	0.391 m	5.91 m
NMPC–DTMPC [19]	0.547 m	11.14 m
NMPC–MPSMC	0.186 m	0.617 m
IAE		
NMPC–NMPC [1]	3.08 m	14.5 m
NMPC–DTMPC [19]	4.00 m	20.0 m
NMPC–MPSMC	1.23 m	4.39 m

assumed known, so $F(x) = 0$. The user-defined constraint sets are $\mathcal{X} = \{|x_1| \leq 0.75 \text{ m}, |x_2| \leq 1 \text{ m/s}\}$, $\mathcal{U} = \{|u| \leq 1 \text{ N}\}$, and $\mathcal{X}_f = Z_f = \{0\}$. System parameters, initial conditions, and weighting matrices are provided in Table 1. Simulations are implemented in MATLAB via direct multiple shooting with CASADI, which includes the nonlinear optimization library IPOPT [30]. The sampling time is $T_s = 0.2$ s with a time horizon of $T = 1$ s. The simulation time is $t = 50$ s.

Closed-loop performance is evaluated using three metrics: the root-mean-square (RMS) values of the states and control input; the integral absolute error (IAE) of the position state; and the integral square error (ISE) of the position state. All metrics are computed as an average over 100 simulations and presented in Tables 2 and 3. Each simulation evaluates at a randomly selected w from within the specified bound. Figure 2 illustrates the trajectories of the states, sliding surface, and the control effort of the system for one realization of the disturbance. As expected, the nominal state stabilizes subject to the tightened constraint, while the true state reaches steady-state offset from the nominal value. The sliding variable does not achieve zero, but it is well bounded within the boundary layer. Finally, the primary controller input is bounded within its tightened constraint, and the auxiliary controller input stabilizes at around -0.2 N.

Another set of simulations were run to investigate the effect of the disturbance bound on the proposed method. An increased disturbance bound of $W = 1.25$ N was considered, with RMS results reported in Table 2 and position and control effort trajectories presented in Fig. 3. It is seen that the amount of disturbance

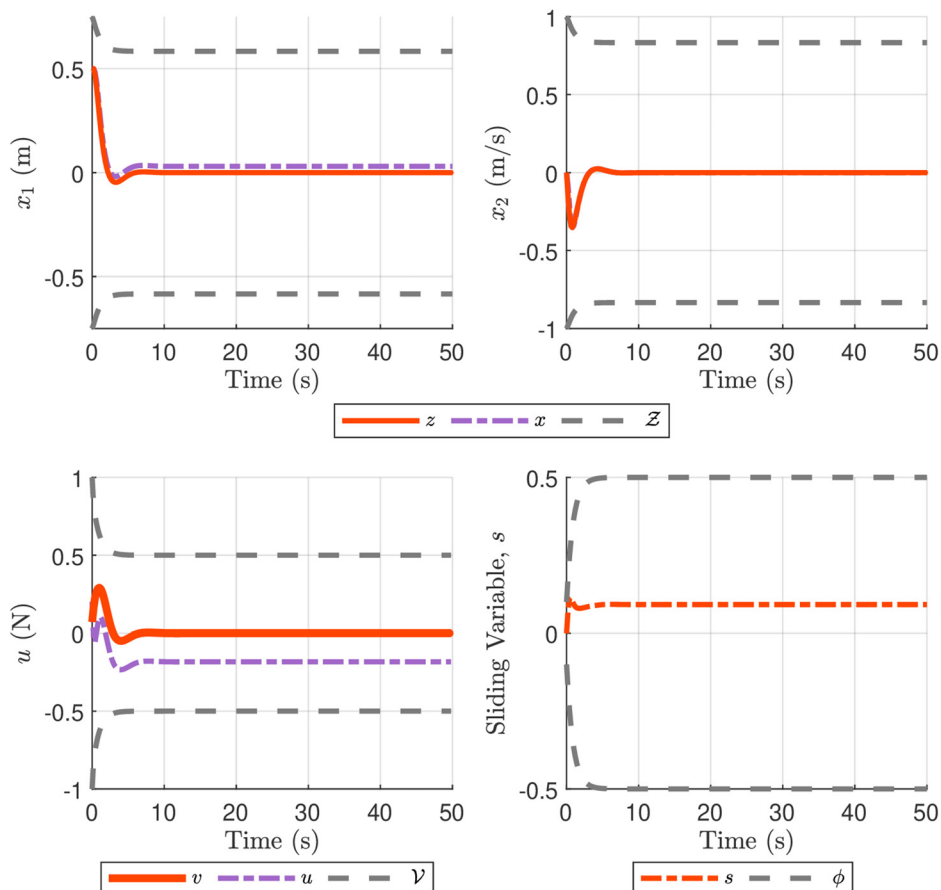


Fig. 2 Plots of nominal and true system trajectories (z, x) with nominal state constraint (Z), the sliding surface trajectory (s) with boundary layer (ϕ), and the nominal and auxiliary control inputs (v, u) with nominal input constraint (\mathcal{V})

minimally impacts the amount of constraint tightening where Z decreases by about 0.1 m and \mathcal{V} remains about the same as a result of the increase in uncertainty from the 0.25 N disturbance bound. From the RMS data, one can see that while comparable levels of state error are achieved between the different bounds, there is a significant increase in the controller RMS. This aligns with traditional concerns on implementing sliding mode control, where decent tracking performance can be maintained in the face of uncertainty at the cost of higher levels of control effort. While the input applied remains well within the constraints, clearly serious consideration must be given between desired tracking performance and input restrictions.

The proposed algorithm is verified against the tube RMPC methods presented in Refs. [1] and [19], referred to here as NMPC–NMPC and NMPC–DTMPC respectively, where the latter controller employs a dynamic tube model predictive controller (DTMPC). These are selected for comparison because the former is a traditional benchmark tube RMPC method while the latter is a tube RMPC method that uses SMC as the auxiliary control, allowing for insight into how encapsulating sliding control under MPC affects system performance. The nominal cost function of NMPC–NMPC employs only the stage cost, identical to $l_{\text{nom}}(z, v)$, while its auxiliary controller cost function is

$$J(x(t_k), \tilde{u}(\cdot)) = \int_{t_k}^{t_k+T} l(\tilde{x}(\tau), \tilde{u}(\tau)) d\tau + V_f(\tilde{x}(t_k + T)) \quad (44)$$

subject to the system dynamics, initial condition constraint, and input constraints, with stage cost $l(x, u) = \|x - z\|_{Q_{\text{NMPC}}}^2 + \|u - v\|_{R_{\text{NMPC}}}^2$ and terminal cost $V_f(x) = \|x\|_{Q_{\text{NMPC}}}^2$, where $Q_{\text{NMPC}} = \text{diag}(50 \ 50)$ and $R_{\text{NMPC}} = 0.5$. The nominal control problem

constraints are $Z = \mathcal{X}$ and $\mathcal{V} = \gamma\mathcal{U}$, where $\gamma = 0.8$ is a scalar that has been tuned to limit constraint violations. The nominal cost function of NMPC–DTMPC is

$$J(x(t_k), \tilde{u}(\cdot)) = \int_{t_k}^{t_k+T} l(\tilde{x}(\tau), \tilde{\lambda}'(\tau), \tilde{u}(\tau)) d\tau + V_f(\tilde{x}(t_k + T)) \quad (45)$$

subject to the system, boundary layer, and tube dynamics, initial condition and terminal constraints, input and state constraints, and additional constraints detailed in Ref. [19], with stage cost $l(x, \lambda', u) = \|x - z\|_Q^2 + \|\lambda'\|_R + \|u\|_R^2$ and terminal cost $V_f(x) = \|x\|_P^2$. The weighting matrices Q , R , and P are identical to those defined in Table 1. The auxiliary controller for NMPC–DTMPC is a boundary layer sliding mode controller that operates with control bandwidth λ' , gain $\bar{K}(x)$ tuned according to Eq. (15), and SMC variables λ and η identical to those in Table 1. Note that the value for the control bandwidth is static for NMPC–MPSMC but a tuned decision variable for the NMPC–DTMPC. With respect to this variable, it is upper and lower bounded for NMPC–DTMPC implementation with user selected values as $0.5 \leq \lambda' \leq 5$. Further, to incorporate the control constraint, NMPC–DTMPC's control input is saturated at 1 N.

The RMS data in Table 2 at $W=0.25$ N reveal that NMPC–MPSMC both maintains the lowest position state error and exerts the most control effort when evaluated against the comparison controllers. Increasing the disturbance bound exacerbates this observation. While both NMPC–NMPC and NMPC–DTMPC increase over three times their initial x_1 state errors as a result of the disturbance increase, the proposed control increases minimally from 0.0722 m to 0.111 m. The data in Table 3 corroborate this observation. The IAE values highlight that the proposed method

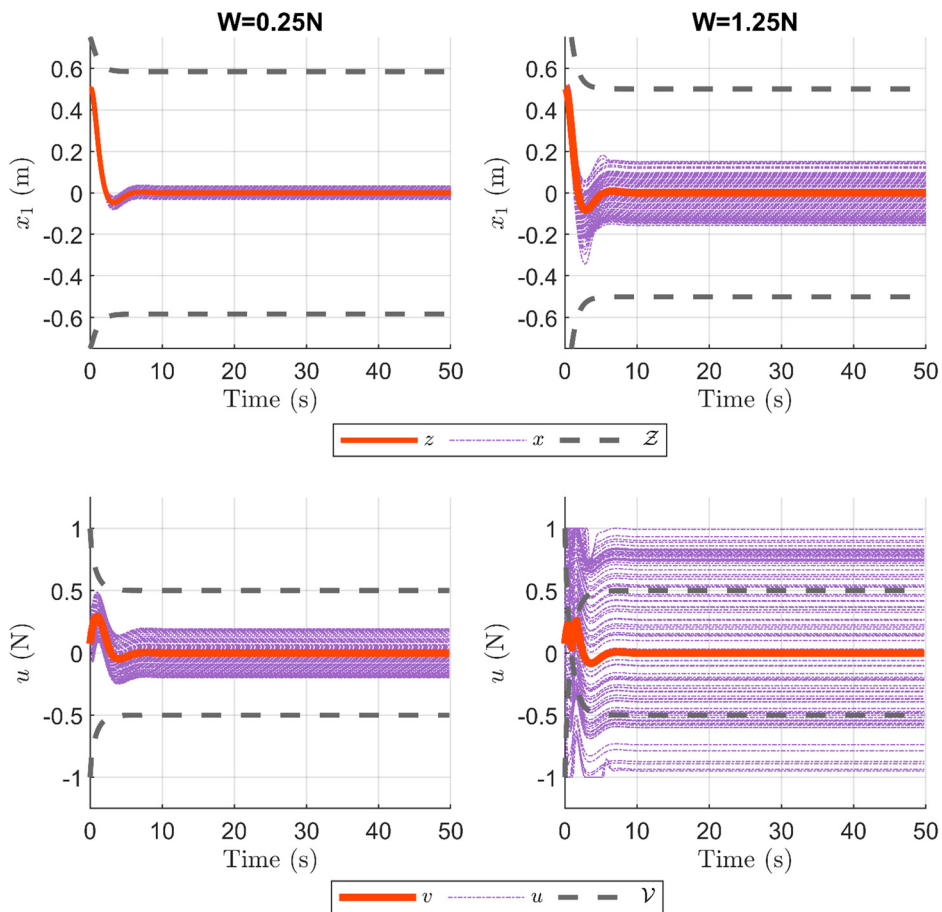


Fig. 3 Plots of the position and control input trajectories for 100 realizations of uncertainty at $W = 0.25$ N (left) and $W = 1.25$ N (right)

maintains the smallest deviation from the origin regardless of disturbance size, while the ISE values indicate that it maintains stronger disturbance rejection properties than the remaining controllers. However, where neither comparison controllers increase in control input by more than about 0.1 N, NMPC–MPSMC increases by over 0.4 N from 0.117 N to 0.510 N for $W = 1.25$ N. That the impact of an increased disturbance bound is considerably higher on NMPC–MPSMC’s control effort than the comparison controllers, especially NMPC–DTMPC which is also SMC-based, reinforces the potential tradeoff between tracking and input requirements in implementing this control design.

The benefit to constraining the SMC auxiliary controller is highlighted in Fig. 4, which displays the phase plots for the system for both NMPC–MPSMC and NMPC–DTMPC. The trajectories in the proposed control remain a safe distance from the extremities of their constraints, while the NMPC–DTMPC trajectories edge close to their x_1 constraint and even violate it on some occasions. Though these violations seem relatively minor, their appearance suggests cases in which an unconstrained SMC can violate the desired state constraint, even while satisfying the input constraint. However, these violations are avoided using a constrained sliding mode controller such as MPSMC for the auxiliary control, offering another tradeoff depending on system requirements.

6.2 Case Study 2: Nonlinear Satellite System. This section considers the stabilization of a nonlinear spacecraft system by the proposed control. The kinematic and dynamic equations of a rigid body spacecraft with reaction wheels in the presence of external disturbances are

$$\dot{q}(t) = \frac{1}{2}\Omega(\omega_b(t))q(t) \tag{46a}$$

$$\dot{\omega}_b(t) = I_b^{-1}[\tau_{\text{ext}}(t) + T_c(t) - [\omega_b(t) \times](I_b\omega_b(t) + Lh_w(t))] \tag{46b}$$

where $q = [q_1 \ q_2 \ q_3 \ q_4]^T$ is the quaternion represented attitude with vector portion $q_{1:3}$ and scalar q_4 , $\omega_b = [\omega_x \ \omega_y \ \omega_z]^T$ is the angular velocity of the satellite body in the body frame, I_b is the moment of inertia of the satellite body represented as a 3×3 matrix, h_w is the reaction wheel angular momentum vector with respect to the body frame, $\tau_{\text{ext}} = [\tau_{\text{ext},x} \ \tau_{\text{ext},y} \ \tau_{\text{ext},z}]^T$ is an external disturbance, $T_c = [T_{c,x} \ T_{c,y} \ T_{c,z}]^T$ is the control torque input, and the operation $\Omega(\omega_b)$, skew-symmetric matrix $[\omega_b \times]$, and reaction wheel distribution matrix for a pyramid configuration L equal

$$\Omega(\omega_b) = \begin{bmatrix} -[\omega_b \times] & \omega_b \\ -\omega_b^T & 0 \end{bmatrix} \tag{47}$$

$$[\omega_b \times] = \begin{bmatrix} 0 & -\omega_z & \omega_y \\ \omega_z & 0 & -\omega_x \\ -\omega_y & \omega_x & 0 \end{bmatrix} \tag{48}$$

$$L = \begin{bmatrix} a & -a & 0 & 0 \\ b & b & c & c \\ 0 & 0 & d & -d \end{bmatrix} \tag{49}$$

where the constraint $a^2 + b^2 = c^2 + d^2 = 1$ applies and the values are defined by $a = b = c = d = 1/\sqrt{2}$. The system’s state and control vectors are $x = [q \ \omega_b]^T$ and $u = [T_c]^T$. The state error

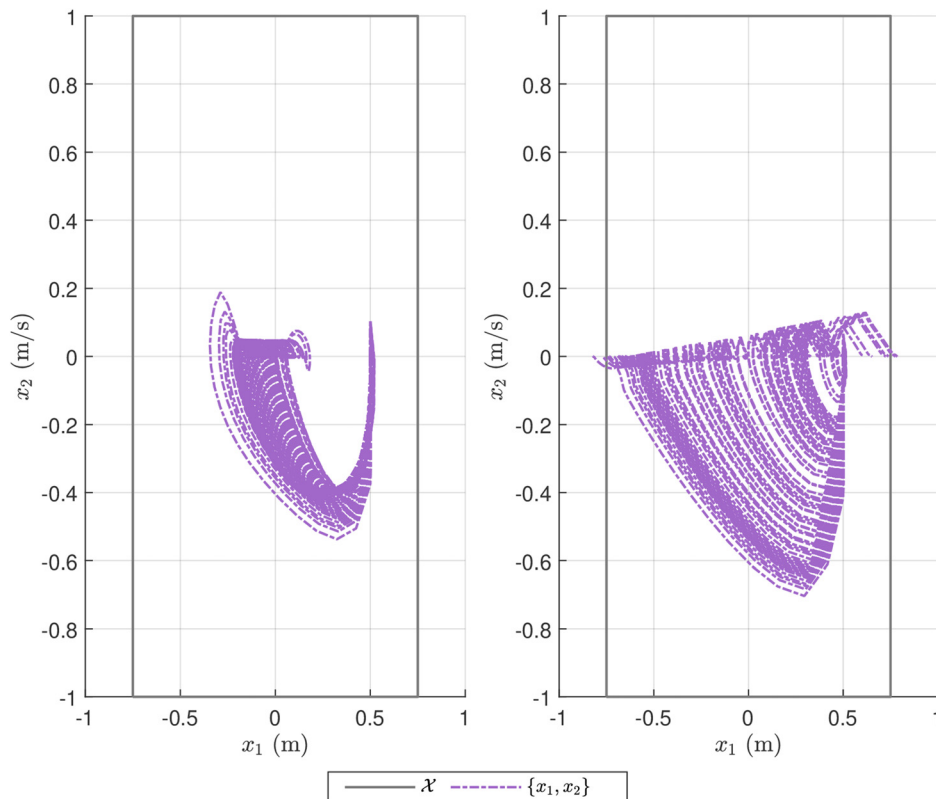


Fig. 4 Plot of the original state constraint (\mathcal{X}) and the true state evolutions ($\{x_1, x_2\}$) for NMPC-MPSMC (left) and NMPC-DTMPC (right)

dynamics, necessary for sliding mode implementation, can be described by

$$q_e = q \otimes q_d^{-1} \quad (50)$$

$$\omega_e = \omega_b - \omega_d \quad (51)$$

where q is the measured quaternion, q_d is the desired quaternion, ω_b is the measured angular velocity of the body, ω_d is the desired angular velocity of the body, and the operator $q \otimes$ represents

$$q \otimes = \begin{bmatrix} q_4 \mathbb{I}_3 - [q_{1:3} \times] & q_{1:3} \\ -q_{1:3}^T & q_4 \end{bmatrix} \quad (52)$$

where \mathbb{I}_3 is a 3×3 identity matrix, and $[q_{1:3} \times]$ is identical to Eq. (48) using the quaternion vector components. The sliding surface for the system is defined by

Table 4 RMS values: nonlinear satellite

State RMS	Controller		
	NMPC-NMPC [1]	NMPC-DTMPC [19]	NMPC-MPSMC
ϕ (rad)	0.0868	0.0714	0.0726
θ (rad)	0.100	0.0876	0.0942
ψ (rad)	0.111	0.0768	0.0791
ω_x (rad/s)	0.00465	0.00299	0.00312
ω_y (rad/s)	0.00454	0.00336	0.00344
ω_z (rad/s)	0.00387	0.00296	0.00309
Control RMS	NMPC-NMPC	NMPC-DTMPC	NMPC-MPSMC
$T_{c,x}$ (N·m)	0.0924	0.0963	0.0833
$T_{c,y}$ (N·m)	0.0895	0.0986	0.0820
$T_{c,z}$ (N·m)	0.0734	0.0904	0.0780

$$s = \omega_e + \lambda q_{e,1:3} \quad (53)$$

The new weighting matrices Q , R , and P , used in all controllers, are now equivalent to $Q = P = \text{diag}(10^2 \ 10^2 \ 10^2 \ 10^{-2} \ 10^0 \ 10^0 \ 10^0)$ and $R = 2\mathbb{I}_3$. Further, the NMPC-MPSMC auxiliary weighting matrices are $Q' = P' = 5 \times 10^4 \mathbb{I}_3$. The updated NMPC-NMPC gains are $Q_{\text{NMPC}} = \text{diag}(10^3 \ 10^3 \ 10^3 \ 10^{-2} \ 10^0 \ 10^0 \ 10^0)$ and $R_{\text{NMPC}} = 0.5\mathbb{I}_3$, and γ remains unchanged. For the SMC-based methods, the control bandwidth λ' and its upper and lower bound remain unchanged, while now $\lambda = 0.015$ and $\eta = 0.03$.

The numerical simulation for the satellite system considers stabilization to the state vector $x = [0 \ 0 \ 0 \ 1 \ 0 \ 0 \ 0]^T$. As done in Case Study 1, the value of the disturbance is randomized but satisfies an upper bound selected as $\tau_{\text{ext,max}} = 3 \times 10^{-6}$ N·m, and the system is assumed known with inertia matrix $I_b = \text{diag}(399 \ 377 \ 377)$ kg m². The constraint sets are

$$\begin{aligned} \mathcal{X} = \{ & -0.225 \leq q_1 \leq 0.1503, -0.1503 \leq q_2 \leq 0.225, \\ & -0.225 \leq q_3 \leq 0.1503, 0.936 \leq q_4 \leq 0.9997, \\ & |\omega_b| \leq 0.05 \text{ rad/s} \} \\ \mathcal{U} = \{ & |u| \leq 1 \text{ N} \cdot \text{m} \} \end{aligned}$$

where the selected state constraint set is based on a pointing constraint of $\pm\pi/8$ rad of the origin for the roll, pitch, and yaw axes, and the control constraint is based on reasonable torque values available for satellite systems. Again, a zero terminal constraint is implemented. The control constraint is incorporated into the NMPC-DTMPC by saturating its control input at 1 N·m. Initial quaternion values are randomized within the constraints defined above, and the initial body angular velocities are set to 0.01 rad/s across all axes. The sampling time is $T_s = 0.4$ s with a time horizon of $T = 8$ s. The simulation time is $t = 7.5$ min. Again, the average RMS over 100 simulations is presented for the states and

Table 5 Integral error values: nonlinear satellite

Position state ISE	Controller		
	NMPC–NMPC [1]	NMPC–DTMPC [19]	NMPC–MPSMC
ϕ (rad)	3.17	3.01	3.13
θ (rad)	3.27	3.18	3.18
ψ (rad)	5.04	3.87	4.03
Position state IAE	Controller		
	NMPC–NMPC	NMPC–DTMPC	NMPC–MPSMC
ϕ (rad)	29.8	29.3	29.7
θ (rad)	30.6	29.9	30.3
ψ (rad)	38.5	34.3	34.6

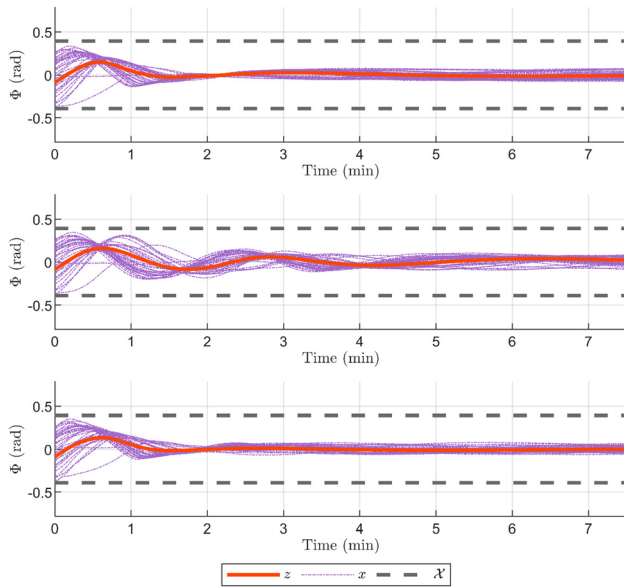


Fig. 5 Plot of true system trajectories (x) along the roll (Φ) axis for 100 realizations of uncertainty with the averaged nominal (z) roll system trajectory and state constraint (λ) across controllers: from top, NMPC–MPSMC, NMPC–NMPC, and NMPC–DTMPC

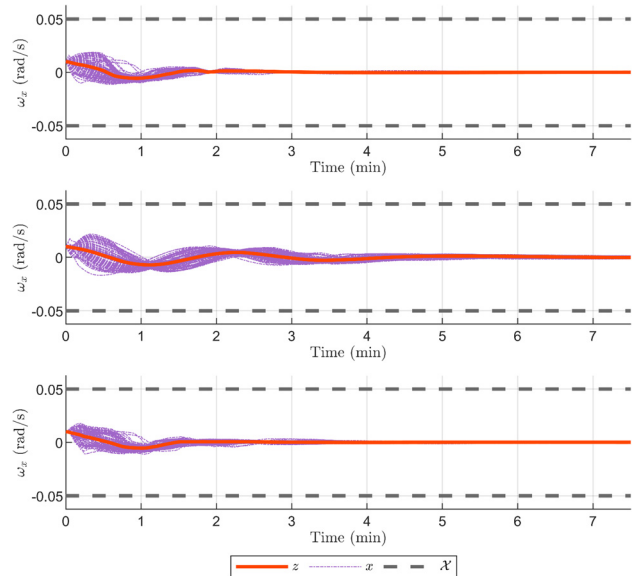


Fig. 6 Plot of true system trajectories (x) for the body angular velocity along the roll axis (ω_x) for 100 realizations of uncertainty with the averaged nominal (z) body roll velocity system trajectory and state constraint (λ) across controllers: from top, NMPC–MPSMC, NMPC–NMPC, and NMPC–DTMPC

controls, while the average ISE and IAE are presented for the position states. The attitude is reported in terms of Euler angles, determined by a 3–2–1 Euler angle rotation into the body frame.

Tables 4 and 5 display the resulting RMS, ISE, and IAE data, which are fairly consistent across state errors and controls for all controllers. Indeed, in terms of the RMS, the proposed approach and NMPC–DTMPC perform comparably, with the latter consistently outperforming NMPC–MPSMC in all categories except RMS for control effort. Further, although the traditional NMPC–NMPC has higher RMS values than the SMC-based techniques in all categories except yaw control effort ($T_{c,z}$), the metrics for all controllers are about the same, highlighting that the proposed approach can perform as well as currently established techniques.

Where the numerical data show nearly identical performance, an examination of the state and control evolutions over time reveals more nuanced information about controller behavior. Figures 5–7 display the state and control trajectories along the roll axis among controllers for the 100 simulations. As shown, the SMC-based tube techniques settle faster than and maintain a tighter spread of trajectories than NMPC–NMPC, each settling around 2.5 min and which is most noticeably observed in Fig. 6.

The most notable difference in performance, however, is in the control effort trajectories displayed in Fig. 7. Not only do the

controls produced by NMPC–MPSMC converge quickly to the nominal trajectory at around 2 min but they are also very smooth for the entire trajectory. Alternatively, both NMPC–NMPC and NMPC–DTMPC display chatter-like motion once they have converged to their nominal trajectories, with NMPC–DTMPC the more afflicted of the two. It is important to note here that while these control efforts seem to chatter, they are not displaying true chattering behavior, and instead rather sudden increases in control effort that, when plotted over 100 realizations, give the appearance of chatter. In fact, each control trajectory plotted individually is smooth with a prevalence of sharp peaks during the simulation. NMPC–DTMPC contains the most peaks in control effort during the simulation, failing to produce a smoother control effort than both NMPC–NMPC and NMPC–MPSMC. Further, one can observe that NMPC–DTMPC operates near the control constraints often in the beginning of the simulation, reaching the saturation limit early. This is avoided in NMPC–MPSMC, which operates well within the control constraint and with smoother levels of control.

Examining the sliding surfaces along the roll axis for both NMPC–MPSMC and NMPC–DTMPC in Fig. 8 reveals similar behavior, where the latter’s surface trajectories are erratic prior to the 2 min settling toward the origin. Observable here is the impact of incorporating the surface into the model predictive design.

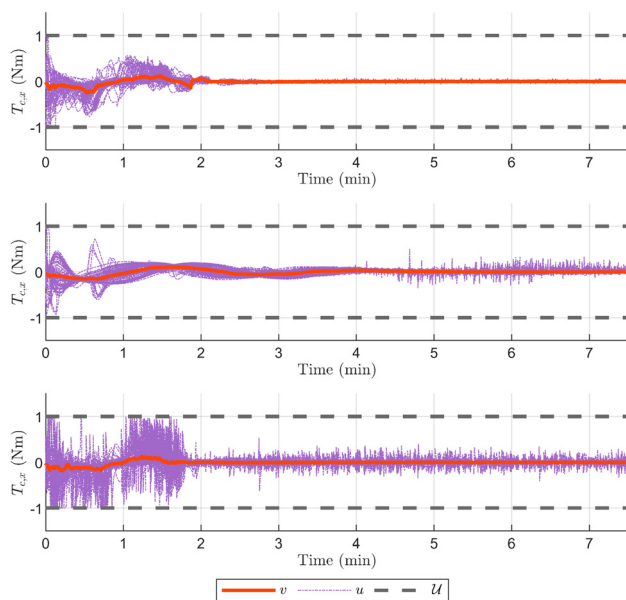


Fig. 7 Plot of auxiliary inputs (u) for the torque along the roll axis ($T_{c,x}$) for 100 realizations of uncertainty with the averaged nominal (v) roll axis torque and input constraint (U) across controllers: from top, NMPC-MPSMC, NMPC-NMPC, and NMPC-DTMPC

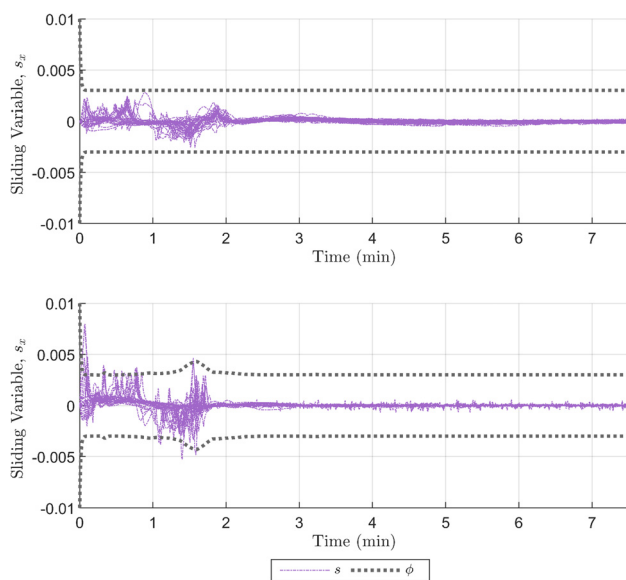


Fig. 8 Plot of sliding trajectories (s) along roll axis states for 100 realizations of uncertainty with the averaged boundary layer size (ϕ) across controllers: from top, NMPC-MPSMC and NMPC-DTMPC

NMPC-MPSMC has a slightly larger spread of trajectories than NMPC-DTMPC after the settling time, affirming the RMS data presented in Table 4 as a tighter spread of s would indicate improved tracking. However, prior to the settling mark, the proposed control has a smaller spread, driven by the MPSMC control to regulate the surface to zero and suggesting lower levels of tracking error during initial target acquisition. Thus, there is merit to incorporating the sliding dynamics into a model predictive design as done in MPSMC, which not only emulates the behavior of a traditional boundary layer SMC while adhering safely to constraints but also more quickly works to regulate the surface trajectories.

7 Conclusions

This paper proposed a tube-based RMPC for continuous-time, nonlinear systems with additive disturbances. A novel auxiliary controller, termed MPSMC, was developed by recasting a boundary layer sliding mode controller as a sampled-data model predictive control problem. This formed a constrained SMC that imbued the control architecture with the robustness properties of sliding mode control without sacrificing constraint satisfaction. As highlighted in the simulation results, by using MPSMC, the developed controller was shown to safely adhere to state and input constraints, unlike NMPC-DTMPC which used the saturated SMC. This demonstrates the importance of employing an SMC that is constrained by design rather than postdesign for use in tube RMPC. Further, the proposed control maintained a tight spread of state and control trajectories similar to or better than NMPC-NMPC and NMPC-DTMPC at varying levels of uncertainty, illustrating its ability to perform comparably to currently used methods. These benefits, however, did come at the cost of elevated levels of control effort for NMPC-MPSMC, which rose considerably as the disturbance bound increased, especially compared to its SMC-based counterpart. Thus, NMPC-MPSMC, more so than other current techniques, confronts the important tradeoff between robust tracking performance and higher levels of control effort. Future work will focus on experimental implementation and incorporating nonadditive forms of uncertainty, including multiplicative and parametric uncertainty.

Nomenclature

- b = system input matrix
- B = user-defined constant
- \mathcal{B} = sliding surface robust control invariant set
- e, e_t = state and tracking errors
- f = nonlinear system function
- F = model error function
- J = open-loop cost function
- k = sample instant index
- \bar{K} = gain value
- l = stage cost function
- L = user-defined constant
- P = terminal state weight matrix
- Q = state weight matrix
- R = control weight matrix
- s = sliding surface
- \mathcal{S} = state error robust control invariant set
- S_0 = tube size
- $\text{sat}(\cdot)$ = saturation function
- t, T, T_s = simulation time, time horizon, sampling time
- u = system control input
- \mathcal{U} = system control constraint set
- v = undisturbed system control input
- \mathcal{V} = tightened system control constraint set
- V_f = terminal cost function
- w = external disturbance
- W = disturbance upper bound
- x = system states
- $\mathcal{X}, \mathcal{X}_f$ = system state constraint and terminal constraint set
- z = undisturbed system states
- $\mathcal{Z}, \mathcal{Z}_f$ = tightened state constraint and terminal constraint set
- $\dot{\cdot}$ = denotes time derivative
- $*$ = denotes optimal solution
- $\hat{\cdot}$ = denotes internal optimization variable
- η = positive constant
- κ = auxiliary controller
- λ, λ' = gain value and control bandwidth
- τ = time sequence over horizon
- ϕ = boundary layer size

References

- [1] Rawlings, J. B., Mayne, D. Q., and Diehl, M., 2017, *Model Predictive Control: Theory, Computation, and Design*, 2nd ed., Nob Hill Publishing, Santa Barbara, CA.

- [2] Song, S., and Wang, J., 2020, "Incremental Model Predictive Control of Active Suspensions With Estimated Road Preview Information From a Lead Vehicle," *ASME J. Dyn. Syst., Meas., Control*, **142**(12), p. 121004.
- [3] Yang, K., and Chen, P., 2021, "Model-Based Predictive Control and Dithering Control for an Integrated Gasoline Engine and Three-Way Catalytic Converter System," *ASME J. Dyn. Syst., Meas., Control*, **143**(9), p. 091007.
- [4] Shaltout, M. L., Ma, Z., and Chen, D., 2018, "An Adaptive Economic Model Predictive Control Approach for Wind Turbines," *ASME J. Dyn. Syst., Meas., Control*, **140**(5), p. 051007.
- [5] Docimo, D. J., Kang, Z., James, K. A., and Alleyne, A. G., 2021, "Plant and Controller Optimization for Power and Energy Systems With Model Predictive Control," *ASME J. Dyn. Syst., Meas., Control*, **143**(8), p. 081009.
- [6] Raković, S. V., Kouvaritakis, B., Findeisen, R., and Cannon, M., 2012, "Homothetic Tube Model Predictive Control," *Automatica*, **48**(8), pp. 1631–1638.
- [7] Raković, S. V., Levine, W. S., and Açikmese, B., 2016, "Elastic Tube Model Predictive Control," *Proceedings of IEEE American Control Conference*, Boston, MA, July 6–8, pp. 3594–3599.
- [8] Fontes, F., Raković, S., and Kolmanovsky, I., 2017, "Rigid Tube Model Predictive Control for Linear Sampled-Data Systems," *Proceedings of 20th IFAC World Congress*, Toulouse, France, pp. 9840–9845.
- [9] Dong, Z., and Angeli, D., 2021, "Homothetic Tube-Based Robust Economic MPC With Integrated Moving Horizon Estimation," *IEEE Trans. Autom. Control*, **66**(1), pp. 64–75.
- [10] Mayne, D. Q., and Kerrigan, E. C., 2007, "Tube-Based Robust Nonlinear Model Predictive Control," *IFAC Proc. Vol.*, **40**(12), pp. 36–41.
- [11] Nikou, A., and Dimarogonas, D. V., 2019, "Decentralized Tube-Based Model Predictive Control of Uncertain Nonlinear Multiagent Systems," *Int. J. Robust Nonlinear Control*, **29**(10), pp. 2799–2818.
- [12] Yan, H., and Duan, Z., 2020, "Tube-Based Model Predictive Control Using Multi-Dimensional Taylor Network for Nonlinear Time-Delay Systems," *IEEE Trans. Autom. Control*, **66**(5), pp. 2099–2114.
- [13] Köhler, J., Soloperto, R., Müller, M. A., and Allgöwer, F., 2021, "A Computationally Efficient Robust Model Predictive Control Framework for Uncertain Nonlinear Systems," *IEEE Trans. Autom. Control*, **66**(2), pp. 794–801.
- [14] Fesharaki, S. J., Kamali, M., Sheikholeslam, F., and Talebi, H. A., 2020, "Robust Model Predictive Control With Sliding Mode for Constrained Nonlinear Systems," *IET Control Theory Appl.*, **14**(17), pp. 2592–2599.
- [15] Rubagotti, M., Raimondo, D. M., Ferrara, A., and Magni, L., 2011, "Robust Model Predictive Control With Integral Sliding Mode in Continuous-Time Sampled-Data Nonlinear Systems," *IEEE Trans. Autom. Control*, **56**(3), pp. 556–570.
- [16] Incremona, G. P., Ferrara, A., and Magni, L., 2017, "Asynchronous Networked MPC With ISM for Uncertain Nonlinear Systems," *IEEE Trans. Autom. Control*, **62**(9), pp. 4305–4317.
- [17] Incremona, G. P., Ferrara, A., and Magni, L., 2017, "MPC for Robot Manipulators With Integral Sliding Modes Generation," *IEEE/ASME Trans. Mechatron.*, **22**(3), pp. 1299–1307.
- [18] Incremona, G. P., Ferrara, A., and Magni, L., 2015, "Hierarchical Model Predictive/Sliding Mode Control of Nonlinear Constrained Uncertain Systems," *Proceedings of Fifth IFAC Conference on Nonlinear Model Predictive Control*, Seville, Spain, pp. 102–109.
- [19] Lopez, B. T., Slotine, J. E., and How, J. P., 2019, "Dynamic Tube MPC for Nonlinear Systems," *Proceedings of IEEE American Control Conference*, Philadelphia, PA, July 10–12, pp. 1655–1662.
- [20] Incremona, G. P., Rubagotti, M., and Ferrara, A., 2017, "Sliding Mode Control of Constrained Nonlinear Systems," *IEEE Trans. Autom. Control*, **62**(6), pp. 2965–2972.
- [21] Garcia-Gabin, W., Zambrano, D., and Camacho, E. F., 2009, "Sliding Mode Predictive Control of a Solar Air Conditioning Plant," *Control Eng. Pract.*, **17**(6), pp. 652–663.
- [22] Hansen, A., and Hedrick, J. K., 2015, "Receding Horizon Sliding Control for Linear and Nonlinear Systems," *Proceedings of IEEE American Control Conference*, Chicago, IL, July 1–3, pp. 1629–1634.
- [23] Rubagotti, M., Incremona, G. P., Raimondo, D. M., and Ferrara, A., 2021, "Constrained Nonlinear Discrete-Time Sliding Mode Control Based on a Receding Horizon Approach," *IEEE Trans. Autom. Control*, **66**(8), pp. 3802–3809.
- [24] Liao, Y., and Hedrick, J. K., 2015, "Robust Model Predictive Control With Discrete-Time Integral Sliding Surface," *Proceedings of IEEE American Control Conference*, Chicago, IL, July 1–3, pp. 1641–1646.
- [25] Fontes, F. A., 2001, "A General Framework to Design Stabilizing Nonlinear Model Predictive Controllers," *Syst. Control Lett.*, **42**(2), pp. 127–143.
- [26] Findeisen, R., Raff, T., and Allgöwer, F., 2007, "Sampled-Data Nonlinear Model Predictive Control for Constrained Continuous Time Systems," *Advanced Strategies in Control Systems with Input and Output Constraints* (Lecture Notes in Control and Information Sciences, Vol. 346), Springer, Berlin, pp. 207–235.
- [27] Slotine, J.-J. E., and Li, W., 1991, *Applied Nonlinear Control*, Prentice Hall, Englewood Cliffs, NJ.
- [28] Magni, L., Raimondo, D., and Allgöwer, F., eds., 2009, *Nonlinear Model Predictive Control: Towards New Challenging Applications* (Lecture Notes in Control and Information Sciences, Vol. 386), Springer-Verlag, Chennai, India, pp. 1–26.
- [29] Landis Markley, F., and Crassidis, J. L., 2014, *Space Technology Library Fundamentals of Spacecraft Attitude Determination and Control*, Springer, New York.
- [30] Andersson, J. A. E., Gillis, J., Horn, G., Rawlings, J. B., and Diehl, M., 2019, "CasADi—A Software Framework for Nonlinear Optimization and Optimal Control," *Math. Program. Comput.*, **11**(1), pp. 1–36.